Mechanisms of estuarine salt plug formation by an along-shelf buoyant current: a numerical model approach

Braulio Juarez[1,2], Arnoldo Valle-Levinson[1], Alberto Canestrelli[1]

Corresponding author: Braulio Juarez (bjuarez@ufl.edu)

Key points

- An along-shelf buoyant current induces an estuarine salt-plug
- Salt-plug formation is independent of the number of inlets in an idealized bay
- Cross-shore winds modifies the circulation produced by the salt-plug

Abstract

While estuarine salt plugs can develop worldwide in estuaries adjacent to buoyant coastal currents, their formation has been scarcely documented. This study aims to generalize a mechanism for salt plug formation that does not invoke evaporation processes but involves a buoyant coastal current modified by wind stresses. A numerical model, Delft3D, is used to simulate two idealized bays, one with a single inlet and another with two inlets. The numerical experiments are inspired by recent observations and simulate nine different scenarios of wind and tidal forcings under the influence of an along-shelf buoyant current. Results show that the salt plug induces an inverse circulation at the inlet with inflow at the surface and outflow underneath. This circulation is modified by wind action. The persistence of the salt plug depends on tidal flushing, as well as wind intensity and direction. A yearlong numerical experiment with non-stationary buoyant currents and non-stationary winds indicate that: (i) onshore winds transport oceanic waters into the bay, while offshore winds export estuarine water to the ocean; (ii) onshore winds enhance the inverse circulation at the inlet, while offshore winds stall it. The ratio between wind-driven and density-induced accelerations, given by the Wedderburn number, determines the dominant contribution to the along-estuary circulation in an along-estuary transect. In general, baroclinicity dominates over wind-stress at the inlet, while wind-stress

[1] Civil and Coastal Engineering Department, University of Florida

[2] Instituto de Investigaciones Oceanológicas, Universidad Autónoma de Baja California

governs the circulation along the estuary. This study represents the first attempt to identify the role of wind and buoyant coastal currents on the dynamics of salt plug formation.

Plain Language Summary

A local of maximum salinity within estuaries is usually refer as a salt plug because it obstructs the renovation of water, affecting the water quality of the estuary. Salt plugs can develop worldwide in estuaries adjacent to low-salinity coastal currents, however, their formation has been scarcely documented. This study aims to generalize a mechanism for salt-plug formation due to a low-salinity coastal current and modified by wind action. A numerical model, Delft3D, is used to simulate two idealized bays, one with a single inlet and another with two inlets. The numerical model simulates nine different scenarios of wind and tidal forcings under the influence of a low-salinity coastal current. Results show that the salt plug induces an inflow at the surface and outflow underneath. A yearlong experiment with a temporally varying coastal current and wind indicate that: (i) onshore winds transport oceanic waters into the bay, while offshore winds export estuarine water to the ocean; (ii) onshore winds enhance the inflow at the surface and outflow underneath at the inlet, while offshore winds stall it. This study represents the first attempt to identify the role of wind and low-salinity coastal currents on the dynamics of salt plug formation.

1. Introduction

Typical estuarine gravitational circulation consists of outflow at the surface and inflow underneath (Pritchard, 1952, 1956; Hansen and Rattray, 1965). Under particular conditions, an estuary can develop a "salt plug", which is defined as a region of maximum salinity inside the estuary. During salt-plug formation, circulation at the inlet reverses and consists of inflow at the surface and outflow underneath, which is referred to as "inverse circulation". Salt plugs usually occur in estuaries where evaporation rates are equal or higher than the freshwater input (Largier, 2010). In hypothermal estuaries, in which estuarine water is colder than in the adjacent ocean, a salt plug induces an inverse density gradient between mid-estuary and the ocean, and a positive gradient between mid-estuary and the estuary head. Those opposing gradients drive a surface convergence zone in the salt-plug region that increases flushing times and reduces water quality within an estuary (Largier, 2010). For this reason, it is crucial to understand the conditions that favor salt plug formation.

Salt-plug formation may not be exclusive of low-inflow estuaries, where evaporation rates are mostly dominant in causing the plug. In Barataria Bay, Louisiana, USA, Juarez et al. (2020) recently proposed an alternative mechanism for salt-plug formation that prescinds of evaporation. Their observations corroborated numerical results of Li et al. (2011), attributing a local salinity maximum inside the estuary to an along-shore buoyant current that transported brackish water into the estuary. Such transport was modified by the direction of the wind. This formation mechanism also appears in other estuaries. In Willapa Bay, north of the Columbia

River, Hickey and Banas (2003) observed a reversal of the salinity gradient between the mid-estuary and the ocean. Such reversal was induced by the intrusion of the Columbia River plume during downwelling (or onshore wind) conditions. Columbia River plume intrusions were also observed at Grays Harbor (Banas et al., 2009) and Strait of Juan de Fuca (Giddings and MacCready, 2017). Numerical simulations in Plum Island Sound, Massachusetts, showed intrusions of the Merrimack River plume into the sound, inducing local salinity maxima (Zhao et al., 2010). These examples correspond to systems adjacent to prototypical plumes (Horner-Devine et al., 2015). However, other types of plumes may contribute to salt-plug formation at adjacent estuaries, such as the Mississippi River that forms a delta-type plume (Horner-Devine et al., 2015).

The main goal of this study is to generalize the mechanism described in Juarez et al. (2020) by exploring the contribution of each forcing involved in the salt-plug formation. A numerical model is implemented for an idealized domain to address this goal. The idealized model allows us to isolate the effects caused by wind, tides and buoyant coastal currents, all involved in the salt-plug formation. We consider both the case of an estuary with one and two inlets. The two configurations allow extrapolations of the conclusions to systems with more than one inlet.

2. Idealized Numerical Model

2.1 Model setup and initial conditions

The Delft3D-FLOW numerical model is implemented for estuarine flow in an idealized domain, which consists of a typical bar-built bay with a river centered at the bay head (Figure 1). The bay dimensions and the values of the input parameters (e.g., Coriolis parameter, initial

104 salinity, tidal amplitude, wind speed, buoyant current speed, and salinity) were inspired by recent
105 salt-plug observations in Barataria Bay (Juarez et al., 2020). The model domain consists of a
106 rectangular grid with 362 cross-shelf cells and 122 along-shelf cells. The cell size is 250 m. In
107 the vertical, the domain is discretized using three sigma layers. Earth's rotation is considered,
108 and the Coriolis parameter f is set to 7.05 x10^{-5} s^{-1} (29^{o} of latitude). The domain consists of three
109 regions: the shelf region, the riverine region, and the basin (estuary or bay) region (Figure 1).
110 The shelf region is beyond 61 km and has a constant depth of 10 m. The riverine region extends
111 from x = 0 to x = 30 km, has a constant depth of 3 m and a width of 2 km. The basin region
112 ranges from x = 30 km to x = 59 km with a constant depth of 3 m, except in the channels, which
113 are 15 km long and depart from the inlet. The maximum channel depth of 10 m is smoothly
114 connected to the basin depth of 3 m using the Delft3D-QUICKIN module with a smoothing
115 factor of 0.5 and 10 smoothing steps. For more information on the smoothing process, refer to
116 the Delft3D-Flow manual (Deltares, 2014). The basin connects to the shelf by means of 2 km-
117 long inlets (from x = 59 km to x = 61 km). The model time step is 1 min, and the model runs for
118 150 days, except in Experiment 5, where it runs for 365 days (one year). The initial water level is
119 at mean sea level (0 m). An initial salinity of 30 g/kg is prescribed for the entire domain,
120 consistently with the maximum salinity observed at Barataria Bay in Juarez et al. (2020). This
121 initial salinity value only affects the maximum salinity reached in the salt-plug and how long it is
122 sustained. A k-ε turbulence closure model is used to compute eddy viscosities and diffusivities.
123

124 **2.1. Boundary conditions**

125 Four open boundaries limit the model domain (Figure 1). A constant riverine discharge
126 (100 m^3/s) is prescribed at the upstream boundary (x = 0 km) with a logarithmic vertical velocity

127 profile. The ocean boundary is parallel to the coast (x = 90 km). At that location, the water level
128 is prescribed in the form of a 0.1 m amplitude (micro-tidal) diurnal tide. The third and fourth
129 open boundaries are on the shelf and perpendicular to the coast (blue lines in Figure 1). At these
130 boundaries, a Riemann condition is prescribed, which simulates a southward along-shelf buoyant
131 current with a vertically uniform velocity of 0.1 m/s. As for the salinity, it is set to zero at the
132 river boundary (freshwater inflow). It is set to 20 g/kg at the boundaries perpendicular to the
133 coast so that the buoyant along-shore current transports brackish water into the domain. A
134 salinity of 30 g/kg is prescribed at the seaward boundary.
135
136 **2.2.Numerical Experiments**
137 A total of nine numerical experiments were run, in which we assessed the relative
138 contributions of three forcings driving the transport and dispersion of salt in the model domain:
139 along-shelf coastal current, tides, and cross-shore winds. Experiments 1 to 4 consider a single
140 inlet in the axis of the basin (y = 15 km) and an along-shelf buoyant coastal current (Figure 1).
141 The next four experiments, 1T to 4T, consider two inlets with the axis at y = 10 km and y = 20
142 km (Figure 1). Inlets have an opening width of 2 km and a cross-shore length of 2 km. All
143 experiments include an upstream river discharge. Experiments 1 and 1T consider no tide or wind.
144 Interactions between tide and coastal current are simulated in Experiments 2 and 2T.
145 Experiments 3 and 3T include tides and a steady offshore wind of 5 m/s. Experiments 4 and 4T
146 include tides and a steady onshore wind of 5 m/s. The magnitudes of these forcings are similar to
147 the one measured in Barataria Bay by Juarez et al. (2020).
148 Experiment 5 lasts one year and consists of a simulation with non-stationary coastal
149 current and wind. The periodicity of the coastal current and the shift in wind direction are

inspired by the seasonality observed in the Barataria Bay area (Juarez et al., 2020). The coastal current velocity is set to a constant value of 0.1 m/s at the beginning of the simulation under no wind conditions. After day 180, the coastal current is turned off (velocity equal to 0 m/s), and an offshore wind is turned on. After day 273, the coastal current velocity is turned on again to 0.1 m/s, and the wind direction switches to onshore. These conditions persist until the end of the simulation.

2.3.Model Output Analysis

All the outcomes are filtered using a Lanczos low-pass filter with a cut-off period of 48 hrs to remove tidal and inertial oscillations. Hovmöller diagrams are used to describe model-related variables that change in space and time. In this study, the axes of the Hovmöller diagrams represent along-channel distance (x-axis) and simulation time (y-axis). Hovmöller diagrams analyze the temporal variation of the subtidal surface salinity for the entire period. Along-channel (*x*-component) subtidal velocities are drawn near the surface and bottom at a grid point (see Figure 1) at the center of the inlet(s). Finally, we present maps of tidally averaged surface salinity and velocity vectors during periods of inverse circulation at the inlet.

3. Results

Results are presented into three subsections. First, we consider steady scenarios with a single inlet. Then, steady scenarios with two inlets. Finally, we consider an unsteady case with two inlets. Each subsection first presents Howmoller diagrams of salinity distributions, followed by time series of surface and bottom velocities centered at the inlet, and concluding with maps of surface velocity and salinity fields.

3.1.Single Inlet Experiments

Single-inlet experiments show the formation of a salt plug that induces an inverse circulation at the inlet. A Hovmöller diagram of the along-estuary salinity distribution shows a salt-plug formation in all four cases: no tide and no wind (Figure 2a), tide and no wind (Figure 2b), tide plus offshore wind (Figure 2c), and tide plus onshore wind (Figure 2d). After 30 days of simulation, salinity reaches maximum values of ~24 g/kg inside the bay and ~22 g/kg at the inlet in Experiments 1, 2, and 4. The relative maximum of salinity inside the bay lasts ~60 days, with the maximum always located between the bay head (x = 30 km) and the inlet, and with salinity values decreasing through time. From day 90 to the end of the simulation, the along-estuary salinity values decrease from the head, < 12 g/kg, to the inlet > 19 g/kg. In experiment 3 (Figure 2c), a local of maximum salinity inside the bay is not clearly noticeable in the Hovmöller diagram representation as in the surface map discussed below. The maximum salinity > 28 g/kg is observed during the entire simulation and even covering a region in the ocean domain near the bars from x = 61 km to x = 65 km, approximately.

Salt-plug formation affects the circulation at the inlet. During the period in which the salt plug is present, surface, and bottom velocities at the inlet depict an inverse circulation with inflow at the surface and outflow underneath (Figure 3). Inverse circulation disappears in experiment 3, which is forced by tide and offshore wind (Figure 3). The inverse circulation is most vigorous in the case with no tide and no wind (Experiment 1, Figure 3a), reaching values of > 0.2 m/s close to surface and > 0.1 m/s near the bottom. In the case of tide and offshore wind forcing (Experiment 3, Figure 3c), downwind flow persists at the inlet during the entire experiment. In this case, the circulation is positive indicating a possible wind stress dominance

196 over density gradients. This competition between wind stress and density gradients is explored
197 further in section 4.2. The inverse circulation persists longer in Experiment 4 (Figure 2d, tide
198 plus onshore wind) than in Experiments 1 and 2. In Experiment 4, the inverse circulation is
199 present during the entire experiment. However, the inverse circulation after day 90 may be wind-
200 induced because it follows the onshore wind at the surface (inflow) and displays a compensating
201 flow in the opposite direction (outflow) near the bottom.

202 Surface maps of salinity and velocity show the spatial structure of the salt-plug and the
203 associated velocities. Day 44 of the simulation is chosen arbitrarily for these maps because the
204 salt plug is present at that time in all the experiments (vertical line in Fig. 3). The horizontal
205 distribution with no tide and no wind (Figure 4a) indicates a maximum salinity zone of ~24 g/kg
206 that extends between x ~ 40 km and x ~ 57 km. Laterally, this zone expands up to ~10 km. The
207 tidally averaged flow is directed landward at the inlet and slightly deflected northward. Outflow
208 develops at the southern end of the bay with velocities of ~0.1 m/s. At the salt-plug zone,
209 velocities are < 0.05 m/s. By adding tides (Figure 4b) the high salinity zone shows a lateral
210 expansion relative to the case of no tides and winds. Also, tides favor the intrusion, up to x ~50
211 km (10 km intrusion), of a plume of brackish water with salinity ~22 g/kg from the along-shelf
212 current. The high salinity zone reaches salinities up to 24 g/kg inside the bay, where the flow
213 velocity is close to zero.

214 The inclusion of offshore wind and tides induces a high salinity zone inside the bay
215 (Figure 4c). The salt plug under the forcing of tides and offshore wind has the highest salinity
216 values, up to ~30 g/kg. Surprisingly, inflows in correspondence of the salt plug axis are the
217 largest ones in the bay, which contrasts with the near-stagnant conditions at the salt plug for the
218 cases with no wind (Experiments 1 and 2). The direction of the flow within the bay follows

theoretical considerations indicating downwind flow over shoals and upwind flow in the channel (e.g., Csanady, 1973; Wong, 1994). An offshore wind opposes the buoyant coastal current in transporting brackish water into the bay. This response causes relatively high salinity water to remain enclosed and recirculating inside the bay. The experiment with onshore winds (Figure 4d) also develops a salt plug. Similarly to the experiment with offshore winds (Figure 4c), the highest outflows appear in the salt-plug region. Again, the residual circulation inside the bay follows theoretical expectations of wind-driven flows over shoal-thalweg bathymetry. The salinity inside the bay is lower than in the simulation with offshore winds (Experiment 3).

The results indicate that a salt plug may appear from an along-shelf buoyant current that intrudes into a single-inlet system. Whether this buoyant water intrusion may develop in systems with two or more inlets is still unknown. The next subsection explores the features of a salt plug in a bay with an additional inlet, under the same forcing conditions.

3.2.Two-inlet Experiments

Experiments in section 3.1 are repeated for a bay with two inlets. Hovmöller diagrams of surface salinity along the thalweg at both inlets (Figure 5) display similar distributions compared to the single-inlet experiment (Figure 2). The most marked differences are observed in the magnitudes of the velocities and the maps of surface salinity and velocity. The ocean-bay circulation structure changes due to the extra inlet. In general, surface, and bottom velocities are higher than the velocities computed in the case of a single inlet. Bottom and surface along-estuary velocities at the center of the two inlets (dots in Figure 1) show an inverse circulation in Experiments 1T (Figure 6a), 2T (Figure 6b), and 4T (Figure 6d). The inverse circulation that develops under no tide and no wind (Experiment 1T), and with tides (Experiment 2T) lasts less

than the circulation resulting from an onshore wind (Experiment 4T). Offshore wind in Experiment 3T enhances a positive circulation at both inlets with bottom velocities higher than surface velocities at the northern inlet and the opposite at the southern inlet. Moreover, the onshore wind enhances the inflow at the surface, which reaches values up to 0.3 m/s. At the inlets, offshore winds prevent the inverse circulation, and onshore winds enhance and prolong the inverse circulation.

Tidally averaged surface salinity and velocity maps (Figure 7) are shown for day 44 of the simulation (see the vertical line in Figure 6). The experiments with no tide and no wind (Experiment 1T, Figure 7a) and with tide (Experiment 2T, Figure 7b) display a maximum salinity zone in the southern portion of the bay. This zone exhibits a maximum salinity of ~24 g/kg at x ~ 52 km, which is the core of a cyclonic gyre with a radius of ~ 10 km. This cyclonic circulation becomes more evident with tides only (Experiment 2T). Although winds modify the circulation (Experiments 3T and 4T), the salt plug remains in the bay. The influence of offshore wind (Experiment 3T) results in a region of maximum salinity that coincides with the location of the thalweg and is surrounded by relatively low-salinity waters (~26 g/kg). The mean flow fields indicate upwind circulation in the thalweg, and downwind over the shallowest region of the bay. This flow pattern agrees with the classical wind-driven theory and generates a re-circulation trapping salty water inside the bay. Outside the bay, the salinity remains higher than 28 g/kg, and the outflow from the southern inlet of ~0.2 m/s is strong enough to stall the inflow of the brackish water from the buoyant coastal current. Onshore winds (Experiment 4T) cause an accumulation of high-salinity (~25 g/kg) water at the southwestern portion of the bay. The wind blowing from the sea to the bay enhances the transport of low-salinity (~22 g/kg) water from the coastal current. Upwind flow of ~0.2 m/s in the thalweg of both channels opposes weaker (~0.1

m/s) downwind inflow over shoals. This residual flow changes direction approximately 2 km from the inlet. In general, the salt plug was persistent until the water inside the bay was homogenized to brackish water by the steady coastal current.

3.3.Unsteady effects

Here we present the results for experiment 5, for which we prescribe a relaxation in the along-shelf buoyant current that allows oceanic water to enter the bay. Experiment 5 included tides, non-steady wind forcing, and a non-steady along-shelf buoyant current (see section 2.2). This experiment shows the same results as experiment 2T (tides and no wind) until the coastal current is turned off on day 180 (not shown). By day ~180, salinity displays the same along-estuary distribution as the experiment with only tides (Figure 5b), with a salinity of ~ 20 g/kg near the inlet (Figure 8). After day 210 waters with salinity > 20 g/kg enter the bay up to ~15 km from the inlet. Offshore winds favor intrusion of waters with a salinity of 24 g/kg up to 20 km from the inlet. Offshore winds also drive buoyant waters away from the inlet, favoring an upwind flow deeper in the channel that imports oceanic saltier water into the bay. By day 270, the salinity contour of 24 g/kg reaches 10 km into the bay. After day 270, the buoyant coastal current is turned on, trapping salty water (>22 g/kg) inside the bay. By day 280, the salinity in the bay is higher than at the inlet. Onshore winds extend the duration of the salt plug in the bay, which persists until day 330 in the northern inlet and until day 310 in the southern inlet.

Surface and bottom subtidal velocities (Figure 9) centered at both inlets show two reversals in the estuarine circulation. The first reversal occurs similarly to that described for steady forcing with only tides (Experiment 4T). By day 181, when the buoyant current is turned off, the gravitational exchange, or positive circulation, increases from ~0.05 m/s to >0.1 m/s at

the surface and the bottom. Offshore winds enhance the positive circulation at the inlet, increasing the outflow at the surface from ~0.05 m/s to >0.2 m/s, and the inflow at the bottom from ~-0.05 m/s to ~0.2 m/s. The second reversal of circulation occurs when both the onshore wind and the buoyant current are turned on. The onshore wind increases the water velocities up to >0.1 m/s and >0.2 m/s at the surface and the bottom, respectively, and also extends the period of inverse circulation until the last week of simulation.

Figure 10 shows maps of tidally averaged surface flow and salinity for day 257 with no coastal current (black line in Figure 9) and on the day with the highest outflow at the surface (red line in Figure 9). Inside the bay, two regions of maximum salinity formed at y ~ 20 km and y ~ 7 km, for the case of offshore winds with no coastal current (Figure 10a) and onshore winds with a coastal current (Figure 10b), respectively. The salt plug in the northern bay is saltier (~26 g/kg) than in the south (~24 g/kg). Inside the bay, the flow is mostly wind-induced, with downwind velocities over the shoals, upwind velocities in the channels, and outflow at both inlets. When the wind reverses to onshore-directed and the coastal current is turned on, the salinity at the inlet decreases to ~22 g/kg, while the salinity at the inner bay is ~24 g/kg. The circulation inside the bay is still wind-driven, with a ~0.2 m/s inflow at the inlet. Therefore, wind enhances the gravitational circulation at the inlet.

4. Discussion

4.1. The Mississippi River plume scenario

The steady-state experiments depicted in sections 3.1 and 3.2 resemble the scenario in which freshwater pulses from an along-shelf buoyant current affects a single inlet and two inlet

311 system. Our results described a steady buoyant current that homogenized the salinity inside the
312 bay after ~ 90 to 120 days of simulation. In reality, the Mississippi River spawns an unsteady
313 along-shelf buoyant current (the Louisiana Coastal Current), which affects a multiple-inlet
314 system (Barataria Bay). The buoyant coastal current may experience relaxation periods since it is
315 linked to the Mississippi River seasonality (Rouse and Inoue, 2005). Relaxation periods result in
316 a decrease in brackish water intrusion into the bays adjacent to the delta (Juarez et al., 2020),
317 thus increasing the average salinity in the bays. On the northwestern U.S. coast, the fate of the
318 Columbia River plume is also linked to seasonality in wind forcing. During onshore or
319 downwelling wind conditions, the intrusion of coastal plume waters into estuaries located north
320 of the river mouth causes inverse estuarine circulation at the entrance of these systems (e.g.
321 Banas 2009; Hickey and Banas, 2003; Giddings and MacCready 2017). To understand the
322 importance of unsteady effects, in section 3.3 we discussed results from an experiment that
323 considered a non-steady buoyant coastal current and wind variability similar to what has been
324 observed in the Mississippi River delta. Results showed that the buoyant inner-shelf current
325 functions as a trap of salty water inside the bay. Salty waters enter the bay during buoyant
326 current relaxation times. Wind action may enhance or reduce trapping depending on its direction.
327 Offshore winds drive the inner-shelf buoyant waters seaward. Under this forcing, the bay may
328 still import salty water through the thalweg following wind-driven theory (Wong 1994; Geyer
329 1997). Onshore winds enhance the inverse circulation at the inlets and the brackish water
330 transport from the along-shelf current toward the bay. These results agreed with observations
331 described at Barataria Bay in the Mississippi River Delta (Juarez et al., 2020), and the
332 observations and numerical results of the bays to the north of the Columbia River (Hickey and
333 Banas, 2003; Banas et al., 2009; Giddings and MacCready, 2017).

334

335 **4.2. Differences between single inlet and two inlets**

336 Salt plugs are form in both idealized configurations, thus suggesting that salt-plug
337 formation may occur at any system adjacent to a buoyant current independently of the number of
338 inlets. However, single-inlet and two-inlets experiments display differences in the velocities and
339 the surface salinity. The extra opening in the two-inlet experiments increases the magnitudes of
340 tidally-averaged velocities at the inlets with respect to the experiments with one inlet (Figure 3
341 and Figure 6). With two inlets, since the tidal prism per inlet is smaller, a smaller volume of
342 water is exchanged with the sea at each tidal cycle, and smaller instantaneous depth-averaged
343 velocities establish at the inlet. As a consequence, vertical mixing is reduced, which
344 enhances stratification and baroclinic circulations. As a consequence, the tidally-averaged
345 velocities are larger in the two-inlet case. Experiments with two inlets show lower salinity waters
346 than one inlet experiments. The mean of the tidally-averaged surface salinity (Figure 4)
347 calculated for the entire bay domain (bay-averaged) (30 km < x < 60 km) with one inlet,
348 experiments 1, 2, 3, and 4 is 22.63, 23.46, 27.76, and 23.19 g/kg, respectively. Meanwhile, mean
349 salinity for the bay domain with two inlets, experiments 1T, 2T, 3T, and 4T (Figure 7), is 21.52,
350 21.57, 27.60, and 21.74 g/kg, respectively.

351

352 Salt flux through each inlet section computed for experiments with one and two inlets
353 characterizes exchange processes through the salinity transport. Following Lerczak et al. (2006),
354 the subtidal salt flux is defined as:

$$F = \langle \int us \, dA \rangle , \qquad (1)$$

where u is the velocity perpendicular to the inlet, s is the salinity and A is a cross-sectional area. The angled brackets denote a tidal low-pass filter (or tidal averages). For two inlets, the salt flux at the northern inlet is added to the flux at the southern inlet. Differences between the fluxes at the cases with one inlet (F_1) and with two inlets (F_2) are computed ($\Delta F = F_2 - F_1$). In addition, the difference between the bay-averaged surface salinity with one inlet ($\widehat{s_1}$) and two inlets ($\widehat{s_2}$) is calculated as:

$$\Delta S = \widehat{s_2} - \widehat{s_1}, \qquad (2)$$

where the hat, ^, denotes the mean for the entire bay domain. When $\Delta S > 0$, bay-averaged salinity with two inlets is higher than that with one inlet. On the other hand, when $\Delta S < 0$ bay-averaged salinity at two inlets is higher than that with one inlet. All the experiments, but the experiments with offshore wind, show the same relation between salt fluxes and differences in bay-averaged salinities (Fig. 11). When $\Delta F > 0$ (blue line in Figure 11) the salt flux is larger in the experiment with two inlets and coincides with $\Delta S < 0$. When ΔS reaches its minimum (vertical black line in Figure 11), $\Delta F \sim 0$, i.e., the salt flux from the two cases is nearly the same. When $\Delta F < 0$ the salt flux with one inlet is higher than that with two inlets and ΔS tends to decrease. These results explain why the salinities in the cases with two inlets are lower than with one inlet. The salinity transport through the inlets is seaward because salt fluxes are positive in both cases (not shown). Moreover, salt fluxes with two inlets are higher than with one inlet when $\Delta F > 0$, yielding an enhanced seaward flushing of saltier water. Experiments with offshore wind follows different response (Figure 11c). Values of ΔF and ΔS oscillates around zero, meaning that the basin is insensitive to the number of inlets when forced by an offshore wind.

4.3.Wind and density gradients as the dominant forcing

377 The wind role on the buoyant inner-shelf currents and the volume exchange at the inlets is
378 twofold. First, it favors or hinders the transport of brackish water from the inner-shelf into the
379 bay. Second, it enhances or stalls the estuarine circulation. Indeed, wind forcing may dominate
380 over density gradients in causing the observed subtidal circulation. The Wedderburn number
381 (Monismith, 1986; Geyer 1997) can be used as indicator of the relative contribution of the two
382 effects since it is defined as the ratio between the wind-stress and the horizontal density
383 gradients:

$$W = \frac{\tau_y L}{g \Delta\rho H^2}, \qquad (3)$$

384

385 where τ_y is the along-estuary wind-stress component ($\tau_y = 0.04\ Pa$, corresponding to a wind
386 speed of 5 m/s), L is a length scale such as the wind fetch, g is the gravitational acceleration, $\Delta\rho$
387 is the along-estuary density difference, and H is the water depth. Wind-stresses drive the
388 circulation if $log_{10}(W) \gg 0$, and the circulation is driven by density gradients if $log_{10}(W) \ll 0$.
389 Here we compute a local value of W by setting L equal to the grid size and $\Delta\rho$ equal to the
390 density difference between adjacent cells. The $log_{10}(W)$ was calculated for a transect centered
391 at the northern thalweg and presented as a Hovmöller diagram in a similar way as the along-
392 estuary salinity diagrams (see Figures 2, 5, 6, and 10). The Hovmöller diagrams for the southern
393 thalweg showed similar results as the northern thalweg. Hence, we only report the diagrams for
394 the northern thalweg.

395 Density gradients drive the residual circulation at the inlet (x ~ 60 km) in most experiments
396 (Figure 12) because $log_{10}(W) < 0$. In experiments with steady offshore winds (Experiments 3,
397 and 3T; Figure 12a and 12c), wind stress dominates over density gradients in the thalweg (45 km
398 < x < 60 km). At 30 km < x < 45 km, the $log_{10}(W) \sim 0$, with a slight dominance of negative

values. This implies dominance of density gradients. However, wind effects are non-negligible. Experiments with a steady onshore wind (Experiments 4, and 4T; Figure 12b and 12d) also show wind dominance along the thalweg. From the channel end to the bay head (30 km < x < 45 km) there is a narrow region where baroclinic forces dominate the wind stresses ($log_{10}(W) < 0$). From x = 35 km to x = 45 km, the wind stresses dominate over the density gradients due to the high friction of this shallow region (H = 3 m). Baroclinic dominance observed from x = 30 km to x ~ 35 km is linked to the salinity front observed in the Hovmöller diagrams (Figures 2d and 5d).

The experiment with unsteady wind forcing (Figure 12e) showed values of $log_{10}(W)$ consistent with the ones observed for Experiment 3T and 4T (Figures 12c and 12d). From day 180 to 271, when there was no buoyancy current and with offshore wind, the along-estuary distribution of $log_{10}(W)$ was similar to Experiment 3T. Density gradients induced residual circulation from the inlet (x ~ 60 km) to x ~ 55 km, wind-stresses dominated the circulation in the thalweg. A region from the channel end to the bay's head seemed to be slightly dominated by the density gradients. From day 272 to the end of the simulation, when the buoyant current is active and an onshore wind is present, the distribution of $log_{10}(W)$ is similar to Experiment 4T (Figure 12d). Density gradients also dominate the circulation at the inlet (x ~ 60 km). Wind stresses induce the circulation observed in the thalweg. A narrow region at x ~ 45 km is density-driven, followed by another wind-driven region from x ~ 35 km to x ~ 45 km. At the bay's head, from x = 30 km to x ~ 35 km, density gradients induce the residual circulation.

This analysis determined the spatial distribution of the dominant drivers of the along-estuary circulation. In the thalweg, the velocity directions followed the wind-driven circulation, with an upwind flow in the channel where density gradients were small. At the inlet, the observed circulation was density-driven and modified by wind stresses.

5. Conclusion

The key finding of this study is that an estuarine salt plug can be formed by an along-shelf buoyant current by modifying the circulation between a semi-enclosed basin and the adjacent ocean. The trapped water forms a salt plug and induces an inverse circulation at the inlet. The salt-plug formation occurs independently of whether the basin has one or two inlets. Such salt-plug formation has been observed in other estuaries where evaporation rates may be neglected.

Wind forcing plays a secondary role that enhances or hinders the salt-plug formation. Offshore winds drive the buoyant current seaward and set up a circulation that allows inflow of salty water into the channel. Onshore winds enhance the transport of brackish waters into the bay, increase the trapping of salty water, and strengthen the inverse circulation at the inlet.

The numerical results described in this study set a baseline to explore the mechanisms of estuarine salt plug formation through a buoyant along-shelf current. This study may be extended in four possible directions. First, the number of inlets could be increased, although we expect that a bay with multiple (>2) inlets should produce similar results, also, the sensitivity to the geometry and depth should be investigated. Second, the ratio between along-shelf current velocities and upstream freshwater velocities should be varied, since this would affect the conditions needed to trap salty water inside the bay. Third, more experiments can be designed to find the different wind conditions that favor salt plug formation or, on the contrary, prevent its formation even in the presence of a buoyant current. Fourth, tidal forcing in this study was small (amplitude = 0.1 m) to represent specific conditions in Barataria Bay (Juarez et al., 2020).

444 Therefore, future studies should investigate the impact of increased tidal flushing on salt plug
445 formation.

446

447 **Acknowledgments**

448

449 This study was funded by the National Science Foundation project (OCE-0825826, OCE-
450 0825833, and OCE-0825876) and by a grant from The Gulf of Mexico Research
451 Initiative/CARTHE II. Funding for Braulio was provided by CONACYT, Mex., under
452 fellowship No. 439858. The model input files are available at 10.6084/m9.figshare.12374840.

453

454

455 **References**

456

457 Banas, N. S., MacCready, P., & Hickey, B. M. (2009). The Columbia River plume as cross-shelf
458 exporter and along-coast barrier. Continental Shelf Research, 29(1), 292-301.

459 Deltares, D. (2014). Delft3D-FLOW Simulation of Multi-Dimensional Hydrodynamic Flows and
460 Transport Phenomena Including Sediments, User Manual.

461 Geyer, W. R. (1997). Influence of wind on dynamics and flushing of shallow estuaries.
462 Estuarine, Coastal and Shelf Science, 44(6), 713-722.

463 Giddings, S. N., & MacCready, P. (2017). Reverse Estuarine Circulation Due to Local and
464 Remote Wind Forcing, Enhanced by the Presence of Along-Coast Estuaries. Journal of
465 Geophysical Research: Oceans, 122(12), 10184-10205.

466 Hansen, D. V., & Rattray Jr, M. (1966). Gravitational circulation in straits and estuaries, J. Mar.
467 Res., 23, 104-122, 1965.

Hickey, B.M., Banas, N.S. (2003). Oceanography of the US Pacific northwest coastal ocean and estuaries with application to coastal ecology. Estuaries 26,1010–1031.

Horner-Devine, A. R., Hetland, R. D., & MacDonald, D. G. (2015). Mixing and transport in coastal river plumes. Annual Review of Fluid Mechanics, 47, 569-594.

Juarez, B., Valle-Levinson, A., & Li, C. (2020) Estuarine salt-plug induced by freshwater pulses from the inner shelf. Estuarine Coastal and Shelf Science,.232, 106491.

Largier, J. L. (2010). Contemporary issues in estuarine physics, chapter Low-inflow estuaries: hypersaline, inverse, and thermal scenarios. Cambridge University Press.

Lerczak, J. A., Geyer, W. R., & Chant, R. J. (2006). Mechanisms driving the time-dependent salt flux in a partially stratified estuary. Journal of Physical Oceanography, *36*(12), 2296-2311.

Li, C., White, J. R., Chen, C., Lin, H., Weeks, E., Galvan, K., & Bargu, S. (2011). Summertime tidal flushing of Barataria Bay: Transports of water and suspended sediments. Journal of Geophysical Research: Oceans, 116(C4).

Monismith, S. (1986). An experimental study of the upwelling response of stratified reservoirs to surface shear stress. Journal of Fluid Mechanics, 171, 407-439.

Pritchard, D. W. (1952). Salinity distribution and circulation in the Chesapeake Bay estuarine system. J. Mar. Res, 11, 106-123.

Pritchard, D. W. (1956). The dynamic structure of a coastal plain estuary. J. Mar. Res, 15(1), 33-42.

Wong, K. C. (1994). On the nature of transverse variability in a coastal plain estuary. Journal of Geophysical Research: Oceans, 99(C7), 14209-14222.

Zhao, L., C. Chen, J. Vallino, C. Hopkinson, R. C. Beardsley, H. Lin, and J. Lerczak (2010), Wetland-estuarine-shelf interactions in the Plum Island Sound and Merrimack River in the Massachusetts coast, Journal of Geophysical Research., 115, C10039.

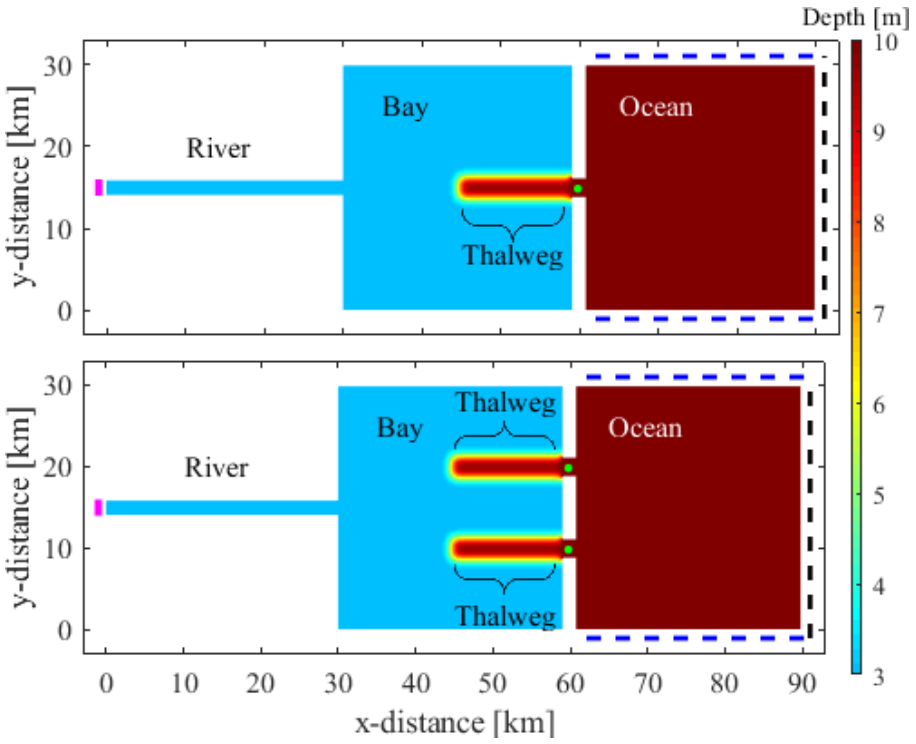

Figure 1. Numerical domain. Upper plot: Domain with a single inlet. Lower plot: Domain with two inlets. The blue dashed lines denote the Riemman open boundaries, black dashed lines denote water level open boundaries, and the magenta lines denote the river discharge boundary. The green dots indicate the locations at which the velocities are sampled (Figures 3, and 6).

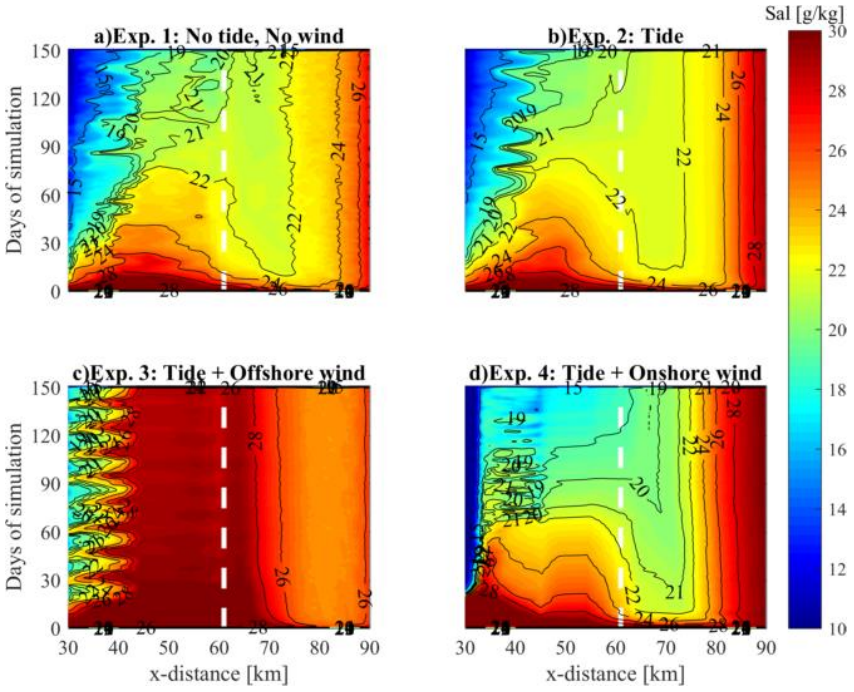

Figure 2. Experiments 1 to 4. Hovmöller diagram of surface salinity in a transect which passes through the channel centerline. Upper plot*:* No wind and no tide (left), and tide, no wind (right). Lower plot*:* With tides plus offshore wind (left), and onshore wind (right). The vertical dashed white line denotes the location of the northern inlet.

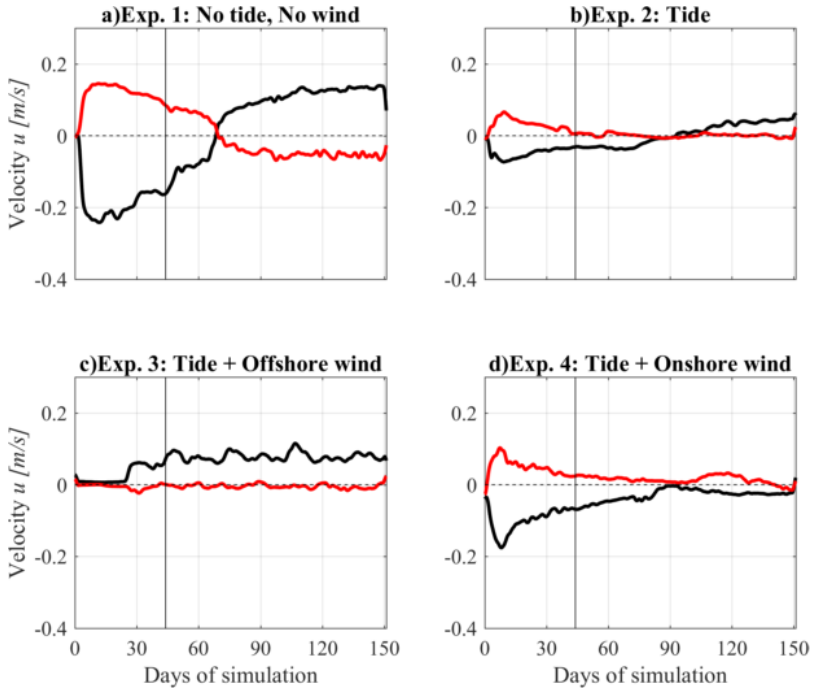

Figure 3. Experiments 1 to 4. Surface (u_s, black) and bottom (u_b, red) subtidal along-estuary velocities centered at the inlet (x ~ 65 km). Velocity is positive seaward. Experiment with no wind is on a) and with a time-varying wind on b) panel. The vertical solid line denotes the time used for Figure 4-7.

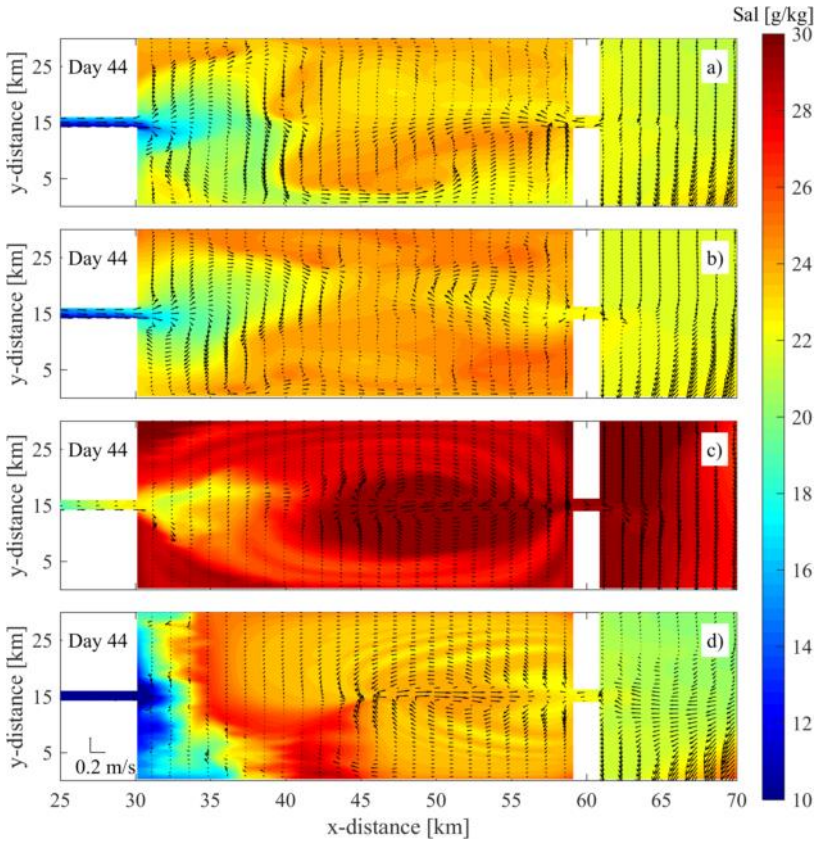

Figure 4. Experiments 1 to 4. Tidally averaged surface fields of salinity (contour colors), and horizontal velocity (arrows).

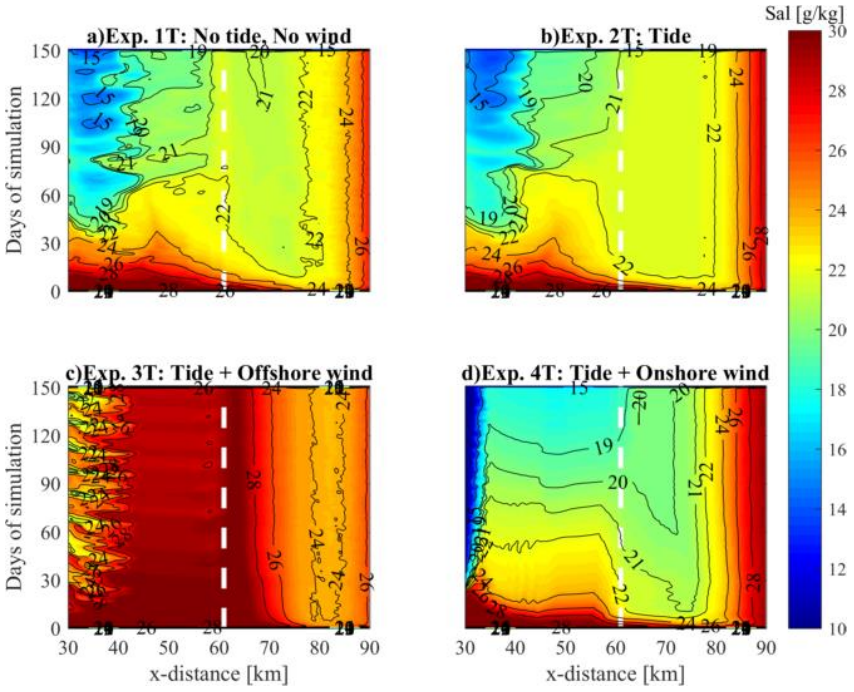

Figure 5. Experiments 1T to 4T. Hovmöller diagram of along-estuary surface salinity centered at the northern channel. a) No wind and no tide, b) tide, no wind, c) tide plus offshore wind, d) tide plus onshore wind, e) tide plus an upwelling favorable wind, and f) tide plus a downwelling favorable wind. The white vertical dashed line denotes the location of the northern inlet.

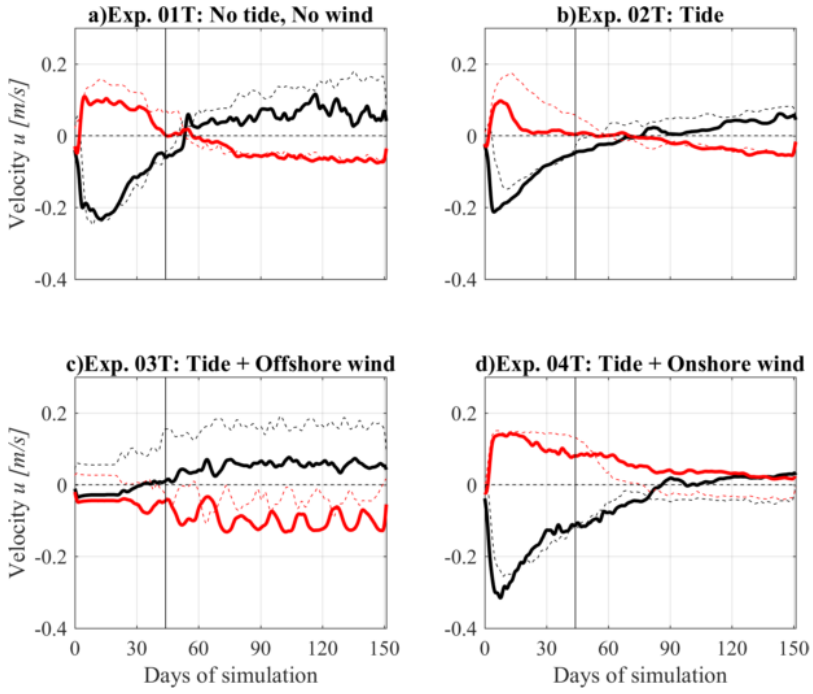

Figure 6. Same as Figure 3 but for experiments with two inlets. Velocity is positive seaward. Surface (black) and bottom (red) subtidal along-estuary velocities centered at the northern (solid lines) and the southern (dashed lines) inlets. The vertical solid line denotes the time used for Figure 7.

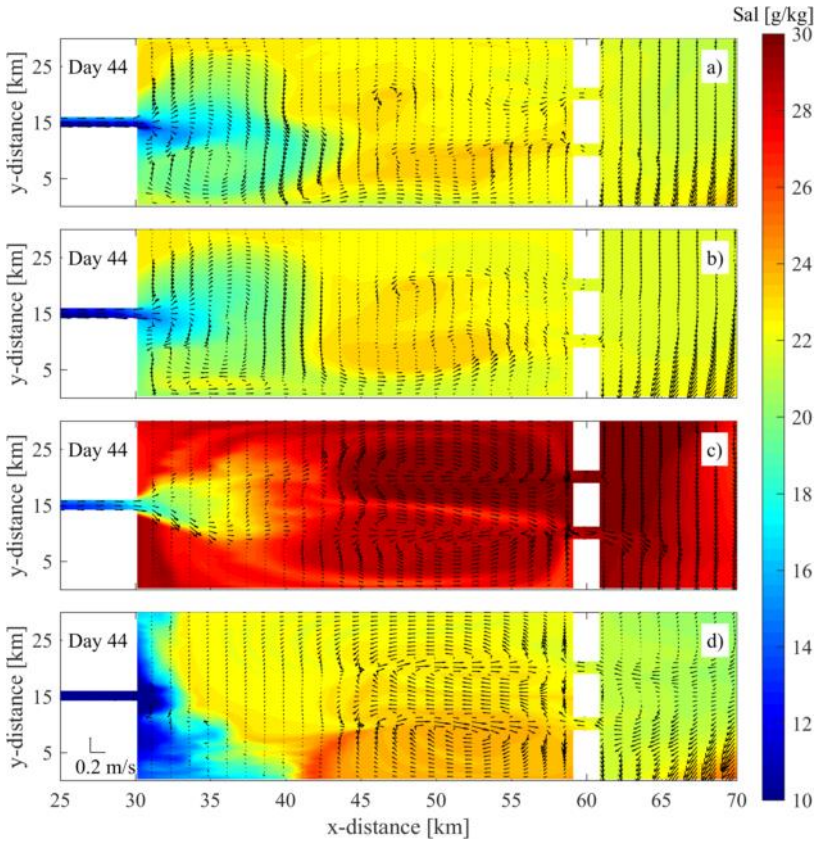

Figure 7. Experiments 1T to 4T. Surface fields of salinity (contour colors), and horizontal velocity (arrows) averaged over one tidal cycle.

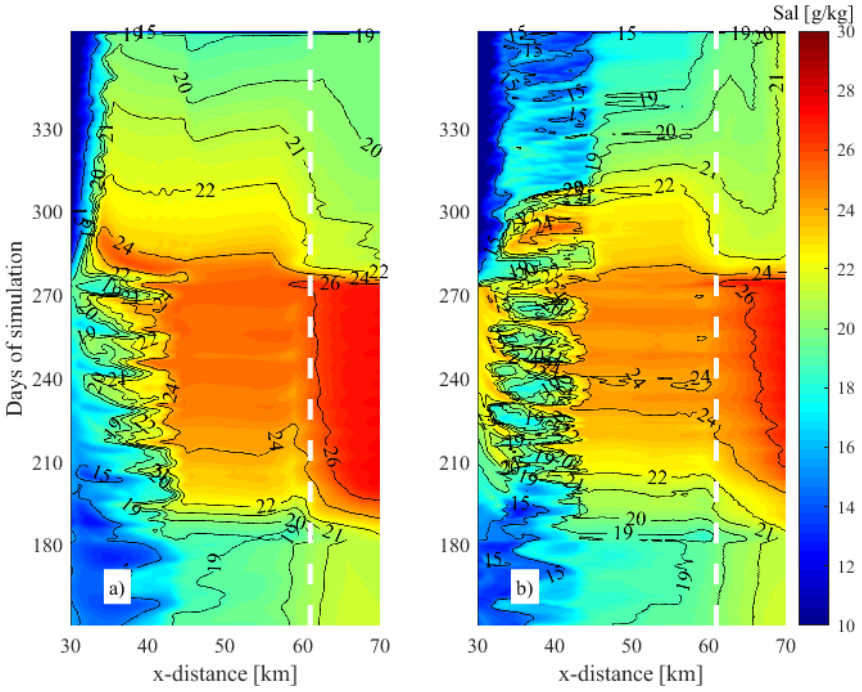

Figure 8. Hovmöller diagrams of along-estuary surface salinity for experiment 5 with the tide and a non-stationary wind for a) northern inlet, and b) southern inlet. The time starts from day 150 because before that time the longitudinal salinity was the same as the experiment only with tides.

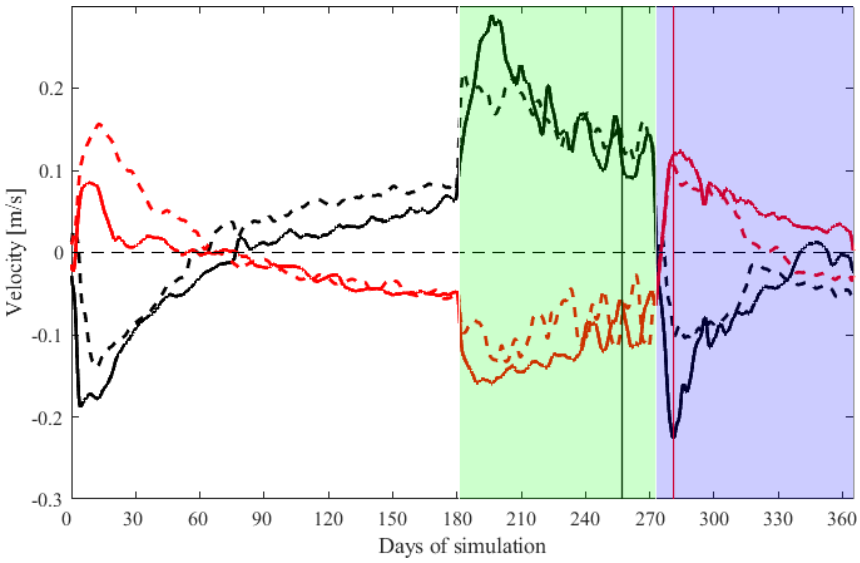

Figure 9. Experiment 5, with tide and a non-stationary wind. Surface (black) and bottom (red) subtidal along-estuary velocities centered at the northern (solid line) and southern (dashed line) inlet during the experiments with a non-stationary coastal current. The green rectangle denotes the period when the buoyant coastal current was turned off and an offshore wind was prescribed. The blue rectangle covers the period when the buoyant current was turned on and the wind direction reversed to onshore. The vertical black and red lines indicate, respectively, simulation day 257 and 281, whose salinity and velocity maps are shown in Figure 10.

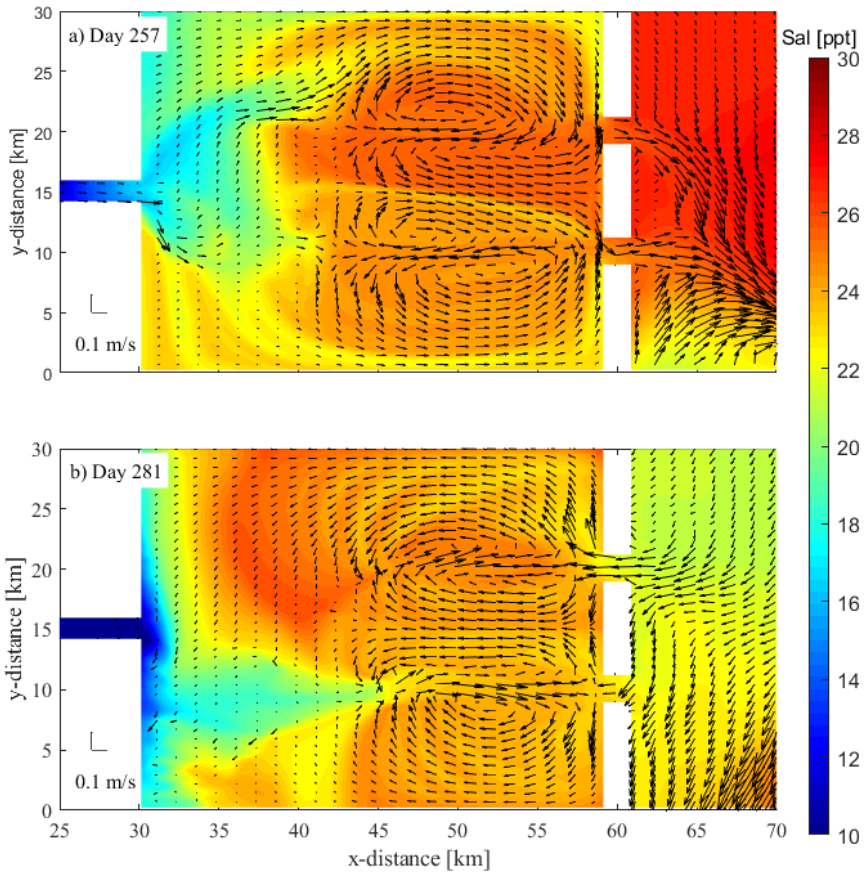

Figure 10. Experiment 5. Surface fields of salinity (contour colors), and horizontal velocity (arrows) averaged over one tidal cycle when the buoyant current was turned off and with offshore wind (a) and when it was turned on and the wind reversed to onshore (b). See Figure 9.

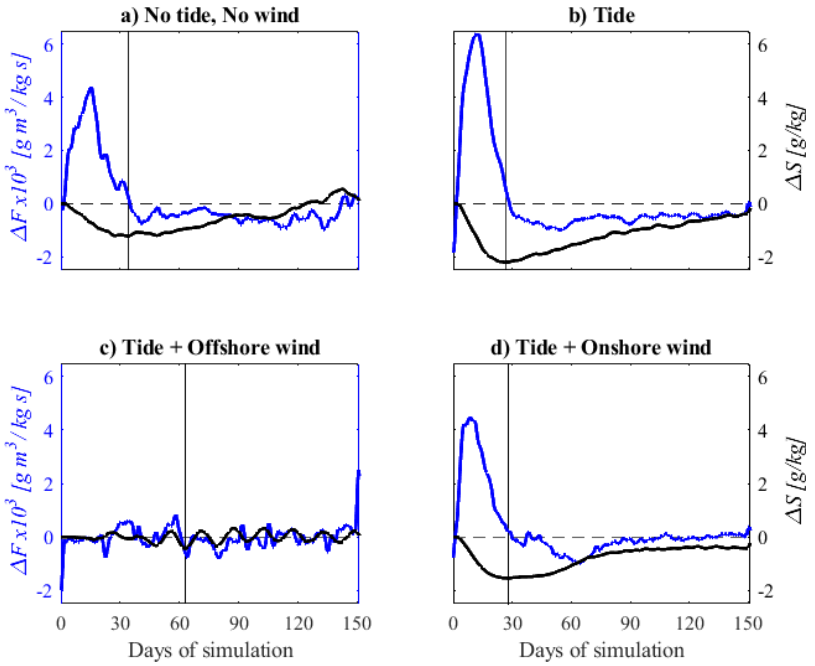

Figure 11. Salt flux difference between cases with two inlets and one inlet (ΔF $[\times 10^3\ g\ m^3/kg\ s]$, blue line) and ΔS $([g/kg]$, black line) for experiments with (a) no tide no wind, (b) with tide, (c) tide and offshore wind, and (d) tide and onshore wind. The vertical black line denotes the time with the minimum ΔS, which coincides with the time when salt fluxes were similar for cases with one and two inlets (i.e., when $\Delta F \sim 0$).

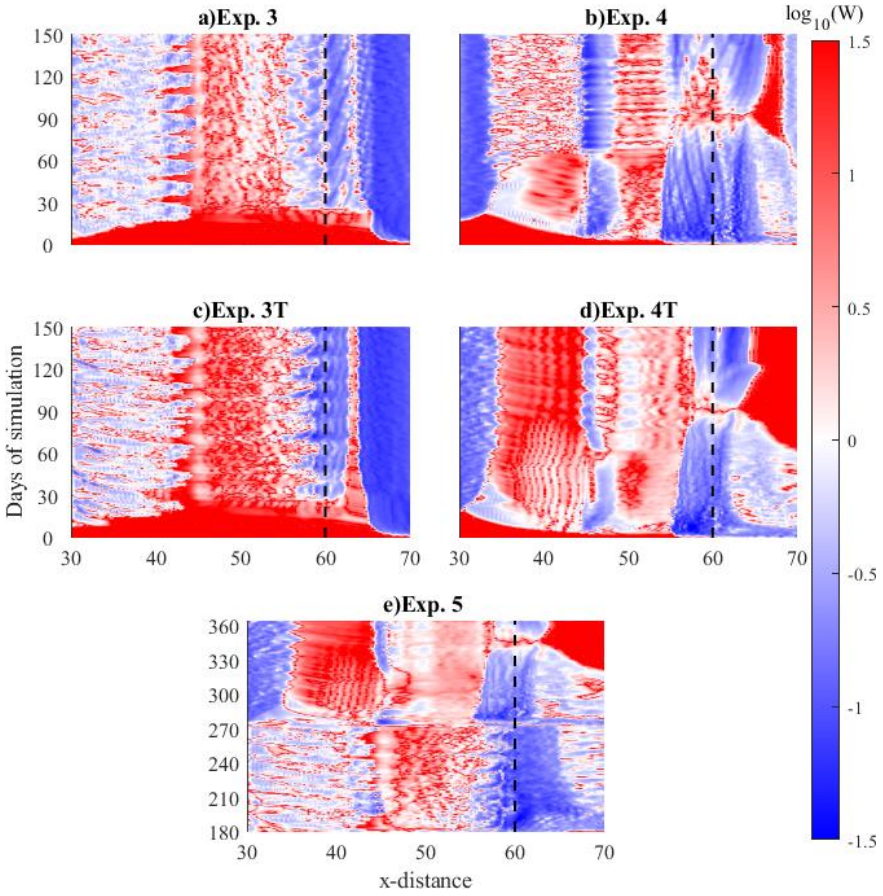

Figure 12. Hovmöller diagrams of the logarithm (log_{10}) of Wedderburn number (W) calculated for experiments with cross-shore wind forcing, centered along the thalweg from the bay head (x = 30 km) to the inlet (x = 60 km, vertical black dashed line). The northern inlet was used for cases with two inlets (Experiments 3T, 4T, and 7, c, d, and e respectively). Blue color denotes $log_{10}(W) < 0$ consequently dominance of the density gradients and red color denotes $log_{10}(W) > 0$ which indicates that wind stresses govern over the density gradients.